Arabian Journal for Science and Engineering (2022) 47:3509–3518
https://doi.org/10.1007/s13369-021-06365-1

RESEARCH ARTICLE-ELECTRICAL ENGINEERING

Analysis of Compact Dual-Band Metamaterial-Based Patch Antenna Design for Wearable Application

Yawar Ali Sheikh[1] · Kashif Nisar Paracha[1] · Sarosh Ahmad[1] · Abdul Rauf Bhatti[1] · Arslan Dawood Butt[1] · Sharul Kamal Abdul Rahim[2]

Received: 4 June 2021 / Accepted: 31 October 2021 / Published online: 26 November 2021

Abstract
A compact dual-band metamaterial-based planar patch antenna on a semi-flexible substrate is analyzed in this article. The design, printed on a Rogers substrate, having a thickness of 3.04 mm and the overall dimension is $70.4 \times 76.14 \times 3.11\text{mm}^3$ ($0.37\lambda_0 \times 0.40\lambda_0 \times 0.016\lambda_0$), where $\lambda_0 = 190$ mm at $f_L = 1.575$ GHz. The design equations are presented for both GNSS (global navigation satellite system) L1/E1 lower band and the upper i.e., 2.45 GHz wireless local area network (WLAN) band. Furthermore, CSRR (complementary split-ring resonator) responsible for the CP (circularly polarized) behavior of the antenna at the lower band is explained using an equivalent circuit model. The proposed equivalent model contains two parallel RLC (resistor-inductor-capacitor) circuits connected in series with one capacitor. To describe its functionality in bending conditions, the antenna is simulated at different bending radii. SAR (Specific absorption rate) of the antenna is evaluated on a voxel human model to check its functionality at different distances from the model. The maximum averaged SAR is found to be 0.381 W/kg at 5 mm from the voxel model. This value is well below the International Commission on Non-Ionizing Radiation Protection (ICNIRP) limit of 2 W/kg averaged over 10 g of human tissue for European countries. The antenna is compared with the literature to show its compactness and superior performance as compared to other already reported designs.

Keywords Dual-band · Wearable antennas · Circularly polarization · SAR

1 Introduction

Metamaterial exhibits many advantages in different applications for different frequency ranges. The geometry of the shape, dimensions, alignment, arrangement of the inclusions determines the nature of the interaction between the metamaterial on host medium and an applied electromagnetic field**.** Metamaterial-based antenna structures are more promising in formation of compact antenna structures with circular polarization characteristics as they have small inclusions which are small compared to the operating wavelength. Moreover, there are no theoretical limits to achieve this compactness except the fabrication limits to realize this structure. A most popular kind of resonator unit cell called CSRR (complementary split-ring resonator) has been proven to miniaturize [1], to empower multiple band operation [2–5], and generation of CP(circular polarization) into patch antennas [6, 7]. The Complementary split-ring resonator exhibits a physical dimension of the order of λ/20, which may represent, a significant limitation. In [1], Compact CP antenna can be created by monitoring the dimensions of the slit of the CSRR to confirm compact size at the cost of marginal peak gain of about -17dBi. The major disadvantage of the structure is that the in-body antenna is the non-polar variety using a coaxial-probe feeding technique which is inappropriate for wearable applications. While on the other side, the proposed work in [8] has shown that the CSSR structure can be printed on the feedline to familiarize the required phase shift, essential to generate two perpendicular electric fields. The phase difference generated between electric field components on the feedline and the ground plane yield in CP radiation properties for the antenna [9, 10].

To ease the design process in order to achieve desired antenna characteristics, LC circuit model of the metamaterial

✉ Arslan Dawood Butt
arslandawood@gcuf.edu.pk

1 Department of Electrical Engineering and Technology, Government College University Faisalabad (GCUF), Faisalabad, Pakistan

2 Wireless Communication Center Faculty of Engineering, Universiti Teknologi Malaysia, Johor Bahru, Malaysia

gives us quick design model. But such models are limited to ideal cases which do not take into account the presence of the dielectric substrate and metallic conductor along with their losses [11]. This problem can be solved by presenting the design equations of the CSRR where the dielectric and conductor losses and behavior have been incorporated as well. The equations not only ease the design process in real scenario but also depicts the complex relationship between the inductances and capacitances presented by the inclusions on the substrate [12]. Since wearable antennas are planned in order to work in proximity to the human body, it is required to address the effects of their radiation characteristics, precisely, in the reactive near field region in the lower frequency band using SAR evaluation at different distances [13]. In the same way, the antenna for this kind of gadget must be combined into a single hardware system, besides conformal, and compact size and operation with minimum coupling effect to the human body [14].

The objective of this research is to give the analysis of the dual-band antenna along with its parametric study, design equations, and an equivalent circuit model. In the Sect. 2, design equations of dual-band antenna have been presented along with an equivalent circuit model of the antenna and a parametric study. In Sect. 3, the bending and human proximity effects have been explained before SAR analysis in Sect. 4. Finally, the antenna has been compared with other standalone solutions for wearable applications to show the compactness of the structure before embarking on conclusive remarks.

2 Design of Dual-band Antenna

The multi-band metamaterial-based patch antenna printed on a semi-flexible substrate is presented in Fig. 1. The Roger substrate RO3003C ($\varepsilon_r = 3$, $\tan\delta = 0.0014$) with a thickness of 3.04 mm was used to fabricate this type of antenna and the overall size is $70.4 \times 76.14 \times 3.11$ mm^3 ($0.37\lambda_0 \times 0.40\lambda_0 \times 0.016\lambda_0$), where $\lambda_0 = 190$ mm at $f_L = 1.575$ GHz) [15]. The design is created on a diamond-shaped patch printed on the substrate i.e., Roger RO3003C, and fed by a Y-shaped EM coupled feedline. In the first design step, the initial size of the patch has been calculated.

In this design, the total peripheral length of the pentagonal patch defines the lower operating frequency band. The operating frequency of the patch can be evaluated using given equations.

$$f_L = \frac{c}{L_T} \tag{1}$$

where, c is called the free-space velocity of light and $L_T = 2L_1 + L_2 + L_3$,L_1, L_2, L_3 are the side lengths of the pentagonal patch (see Fig. 1a). For the design, the total peripheral length equals $L_T = 185.22$ mm with wavelength in free space at the resonant frequency (1.575 GHz) of the patch is λ_{res}

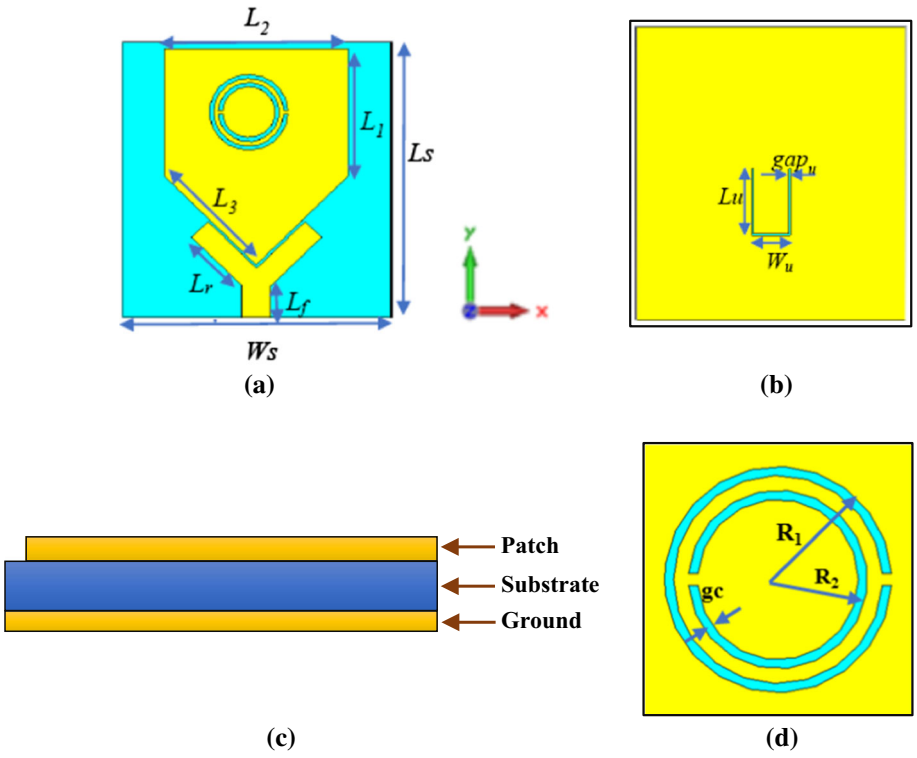

Fig. 1 **a** Front view and layout of the antenna, **b** Back view of the antenna, **c** Side view of the antenna, **d** CSRR unit cell on the patch

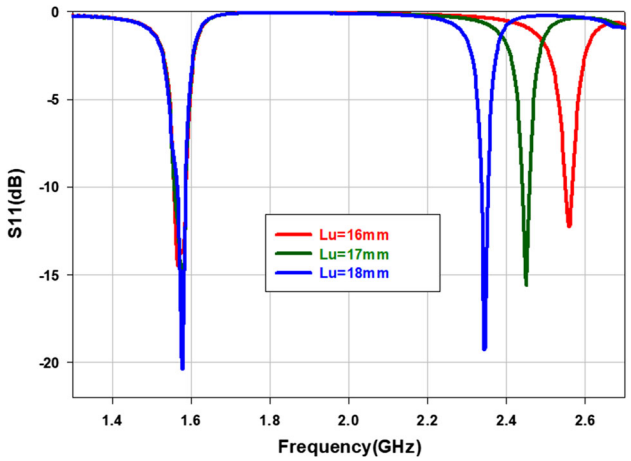

Fig. 2 Effect of U-Slot on S11 (dB)

= 190.3 mm. Hence, as the total patch length is increased the operating frequency shifts toward lower frequency band (Eq. 1).

On the other side, the higher band is perturbed by creating a U-shaped slot on the ground plane (see Fig. 1b). As the U-slot length is increased, the operating frequency shifts toward the lower band. The upper resonance (f_u) can be determined by using the following equation.

$$f_u = \frac{0.4c\sqrt{\varepsilon_r}}{L_{ut}} \tag{2}$$

where ε_r is the relative permittivity of the substrate, and L_{ut} is the total U-slot length. It can be observed from Fig. 2, as the U-slot length increases from 16 to 18 mm, the upper band shifts 2.59 GHz to 2.39 GHz.

2.1 Equivalent Circuit Model of the Dual Band Antenna

An equivalent circuit model is designed in ADS (Advanced Design System) for a dual-band patch antenna operation as can be seen in Fig. 3a. This circuit model is made for the measurement of input impedance matching which is utilized to build an equivalent circuit of dual-band antenna. The proposed equivalent model contains two parallel RLC (resistor-inductor-capacitor) circuits connected in series with one capacitor. The values of inductors, resistors, and capacitors can be seen in Table 1.

In Fig. 3a, it can be observed that two parallel RLC circuits are utilized to achieve dual-band frequencies i.e., 1.55 GHz and 2.45 GHz. In order to get a lower band i.e., 1.55 GHz, one capacitor in parallel with one inductor and one resistor is used. In this portion, by varying the values of L1 and C1 the lower frequency band shifts. In the same way, another parallel RLC circuit is designed to achieve a higher frequency

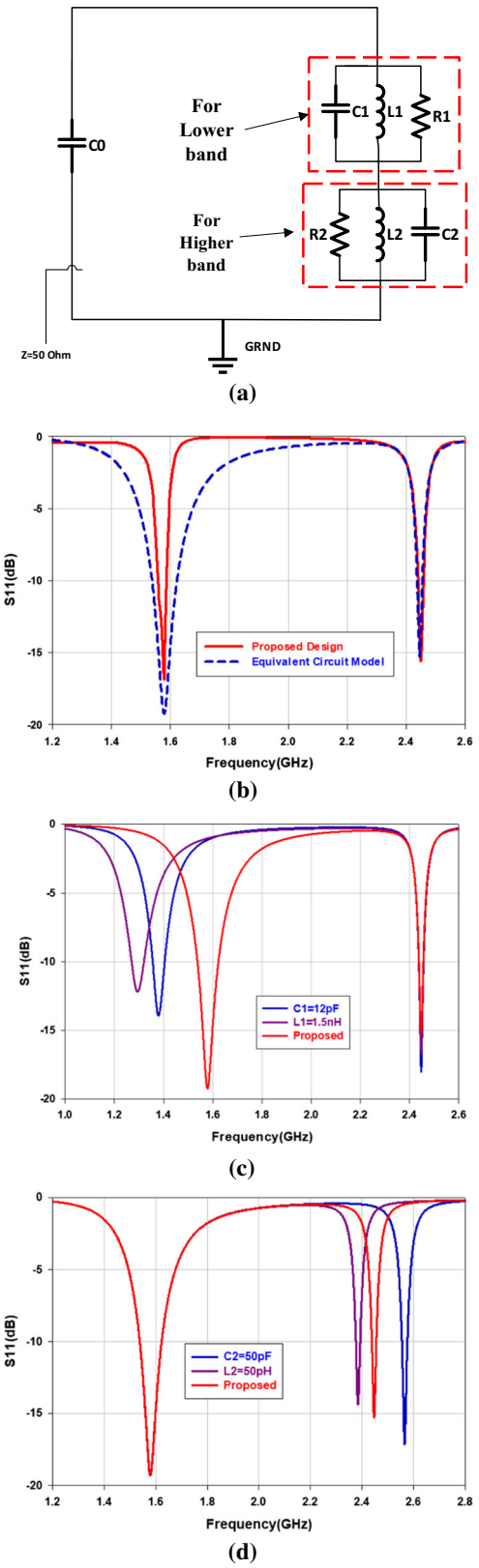

Fig. 3 **a** An Equivalent Circuit Model for the Proposed Design, **b** Comparison of Equivalent Circuit Model with Proposed Design, **c** Lower Frequency Band Optimization in Equivalent circuit, **d** Higher Frequency Band Optimization in Equivalent circuit

Table 1 List of the Values for Equivalent Equivalent circuit

Inductors	Values (nH)	Capacitors	Values (pF)	Resistors	Values (Ω)
L1	1.02	C0	1.5	R1	110
L2	0.076	C1	9	R2	80
Z	50	C2	55		

band i.e., 2.45 GHz. Here, one capacitor in parallel with one inductor and one resistor is utilized. By varying the values of the C2 and L2, the higher frequency band can be tuned. Resistors are used to increase the return loss [dB] to keep it less than 10 dB. Reflection Coefficient [dB] can be improved by decreasing the values of the resistors and vice versa. Comparison of S11 [dB] of equivalent circuit model with proposed dual-band monopole antenna is presented in Fig. 3b**.**

To vary the lower frequency band i.e., 1.55 GHz, the values of L1, and C1 can be varied as presented in Fig. 3c. By increasing the values of C1 the lower band shifted from 1.55 GHz to 1.3 GHz and by increasing the value of L1, the lower frequency band shifted towards 1.38 GHz. While in order to vary the higher frequency band i.e., 2.45 GHz, values of C2 and L2 are varied as shown in Fig. 3d. It is clear from the graph that by increasing the value of C2, the higher frequency band shifted from 2.45 GHz to 2.5 GHz and by increasing the value of L2, the higher band moved from 2.45 GHz to 2.35 GHz.

2.2 Equivalent Circuit Analysis of CSRR

CSRR is a type of metamaterial-based design that offers negative permeability that has an electrical length smaller than the operating wavelength. CSRR, due to its miniaturized size, has been loaded in the patch to shift the resonant frequency towards the lower band and to excite the orthogonal excitation field so as to introduce CP radiations characteristics. The antenna used a complementary split-ring resonator in order to reduce the size and to enable circularly polarized behavior at lower frequency without use of via, opposite to [16], or the double probe feeding techniques presented in [3].

The presence of the split-ring resonator structure instantaneously resulted in 5% extra miniaturization of the antenna structure, in comparison to the diamond-shaped patch radiator without CSRR. The overall size reduction is more than 60% as compared to the antennas proposed in [4, 17] [8] and 14.87% associated with other electromagnetics coupled CP structures [5, 10]. The reported antenna in [4] is sized at 105 mm x 110 mm [$(0.66 \times 0.69\ \lambda_0)^2 = 0.45\ \lambda_0{}^2$ where λ_0 = 157 mm at 1.9 GHz. Whereas the antenna reported in [8] is sized at 80 mm x 80 mm [$(0.64 \times 0.64\ \lambda_0)^2 = 0.4096\ \lambda_0{}^2$], where $\lambda_0 = 124$ mm at 2.45 GHz.

As can be seen from Fig. 4a, the lower band of the design shifted from 1.65 GHz to 1.575 GHz (4.56%) after the inclusion of CSRR while the upper band remained unchanged. By

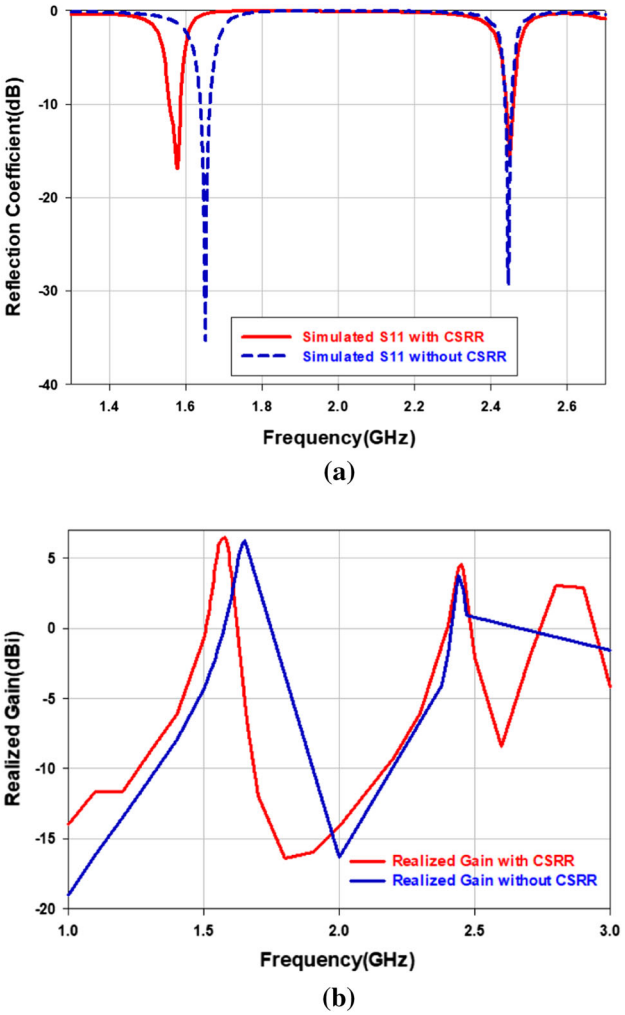

Fig. 4 **a** Effect on reflection coefficient by introducing CSRR into the patch, **b** Realized gain with and without CSRR into the patch

tuning the geometric parameter of CSRR like R_1, g_c, the time phase shift of 90^0 in two modes at 1.575 GHz is generated, which enables the CP radiation characteristics [16]. Furthermore, the simulated boresight gains with and without CSRR depicted in Fig. 4b show that the realized gain remains unaltered by introducing the resonator unit cell in the triangular patch except for a slight shift in the lower band.

The CSRR unit cell's equivalent circuit model is presented in Fig. 5, where the operating band of CSRR can be defined as:

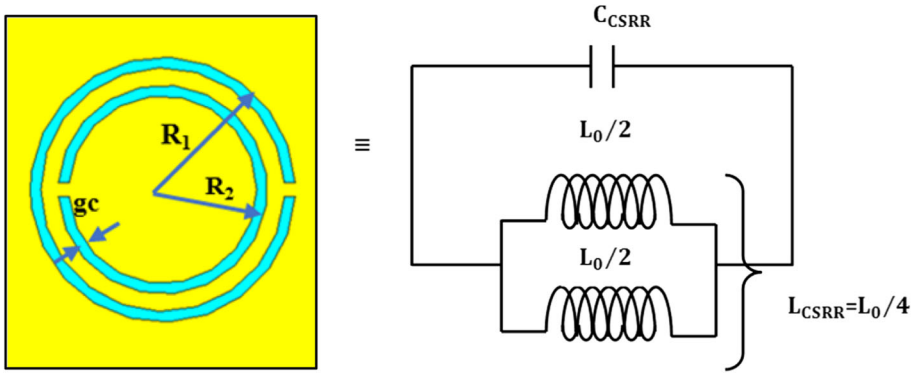

Fig. 5 CSRR topology and its equivalent parallel tank circuit

$$f_r = \frac{1}{2\pi\sqrt{L_c C_c}} \tag{3}$$

where L_c is the inductance of CSRR (due to metallic strips in between the slots), and C_c is the capacitance of the CSRR (due to slots in between the metallic strip).

It has been proven that, in a quasi-static regime, the mutual inductance of the CSRR is not affected due to the existence of the dielectric substrate on which it is fabricated. Hence, inductance can be calculated as under [11].

$$L_c = 2.43\mu_0[l-(N-1)(W+g_c)]\left[\ln\left(\frac{0.98}{\rho}\right)+1.84\rho\right] \tag{4}$$

$$\rho = \frac{(N-1)(W+g_c)}{[l-(N-1)(W+g_c)]} \tag{5}$$

where μ_0 is the vacuum permeability, $N = 2$ is the number of rings in CSRR, $l = \pi R_1/4$ equivalent to the side length of the external ring of the square shape CSRR, $W = R_1 - R_2$ is the width of the metallic strip, g_c is the isolation between two adjacent strips, and ρ is the filling ratio. The expression of the capacitance can be calculated as given below [11].

$$C_c = \frac{N-1}{2}[2l-(2N-1)(W+g_c)]C_0 \tag{6}$$

where C_0 is the reciprocal of unit length capacitance among the equivalent strips and incorporating the effect of height h and relative permittivity ε_r and given by following equation:

$$C_0 = \varepsilon_0\varepsilon_r^{sub}\frac{K\left(\sqrt{1-k^2}\right)}{K(k)} \tag{7}$$

$$\varepsilon_r^{sub} = 1+\frac{2}{\pi}\arctan\left[\frac{h}{2\pi(W+g_c)}\right](\varepsilon_r-1) \tag{8}$$

where ε_0 is permittivity in vacuum, K is the complete elliptical integral of the initial type, $k = g_c/g_c + 2W$, and ε_r^{sub} is relative permittivity linked with the dielectric filling of the substrate. MATLAB code has been written to evaluate the values of inductance and capacitance of CSRR (L = 1.373 × 1013H, C = 8.74 × 108 F) and resonance frequency has been evaluated from Eq. 3. The slits intercepting the annular slots is critical in the generation of the resonant frequency of the CSRR. The above set of equations were suitably employed to obtain the design dimensions of the CSRR's.

2.3 Parameters of the CSRR Affecting Reflection Coefficient and Axial Ratio

As seen in Fig. 6, the center frequency of the AR is descending as the outer radius (R_1) of the CSRR is increased, without the reflection coefficient plot. This is due to the changes in the equivalence inductance and capacitance in the ring of the CSRR unit cell, which eventually changes the mutual phase difference between the patch and the ground at the resonating frequency.

The same effect can be observed by varying the internal radius (R_2) of the circular ring. Next, the effect of the gap between the rings of the CSRR on AR and the antenna's return loss has been investigated, as shown in Fig. 7**.** The optimal AR point shifted towards the higher frequencies with the increase of the gap in the CSRR. However, similar to the previous parameter, the reflection coefficient remained the same.

Hence, it can be concluded that impedance matching at the lower band does not depend upon the parameter of the CSRR, and hence, limiting its effect on the 2nd band. Meanwhile, AR is observed to be more sensitive to its outer radius (R1) than the gap (g_c) and the inner radius (R2). It is observed, as reported in [15], that the position of the slits in the split ring resonators has an impact on the polarization behavior of the design. If the circular slits inside CSRR are cut in the reverse direction of the antenna, the antenna will give LHCP features instead of RHCP.

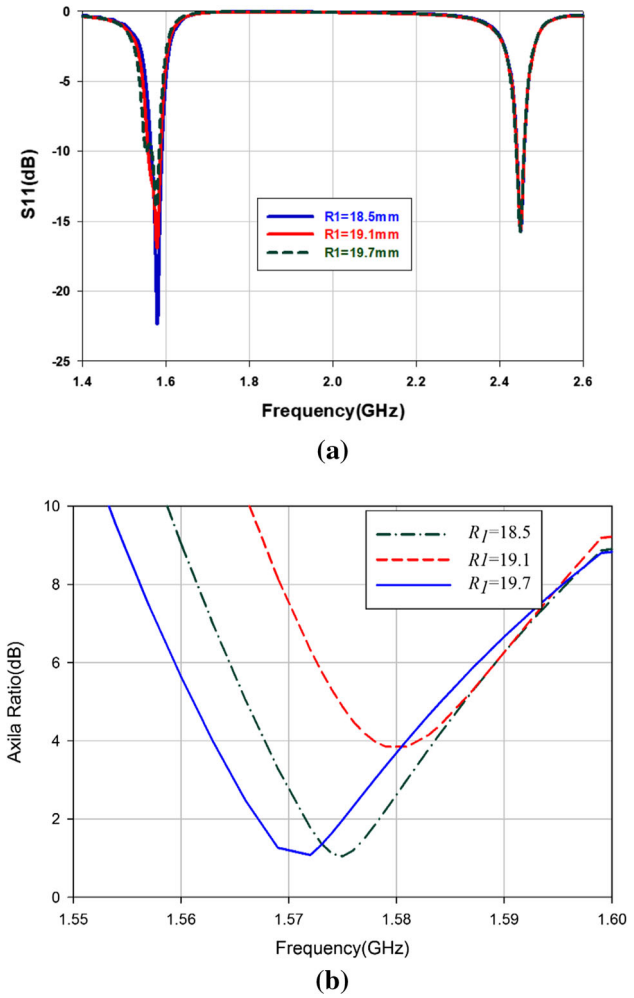

Fig. 6 The effects of the outer radius of CSRR(R_1) on the **a** S11 (dB), **b** Axial ratio

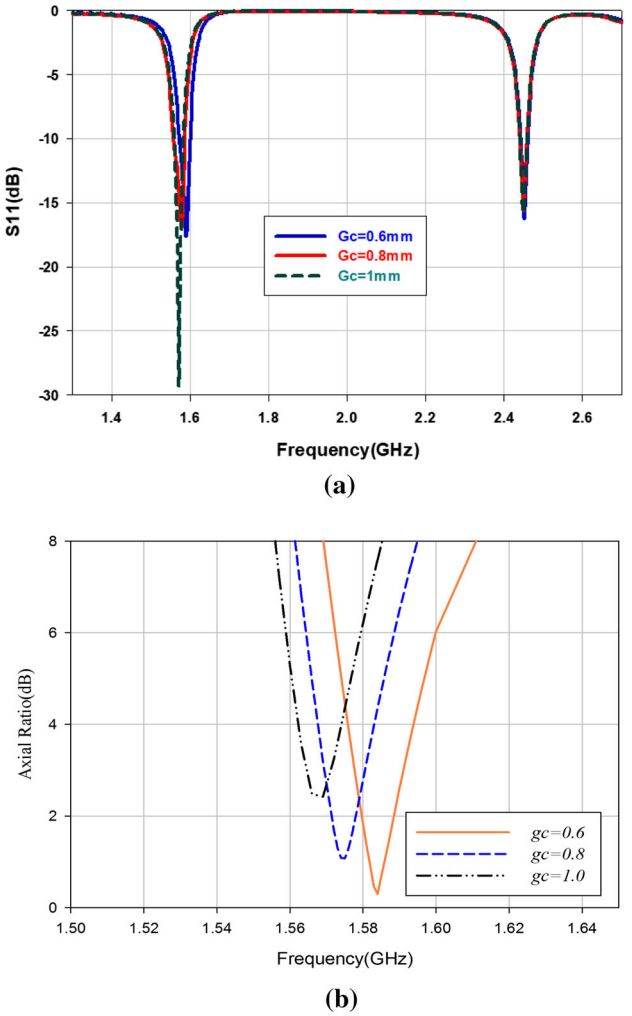

Fig. 7 The effect of gap of CSRR (gc) on the **a** Reflection coefficient(dB) **b** Axial ratio(AR)

3 Study of Bending and Human Proximity Effects

Metamaterial-based wearable antennas suffer from two critical effects. First, the bending of the antenna when being worn, which results in performance degradation especially in terms of reflection and radiation properties [18]. Second, the closeness to the human body which may distort the antenna radiation performance severely [19]. Both aspects are discussed in the following sections.

3.1 Bending Effect on Dual Band Antenna

Wearable antennas are typically made using flexible materials, and due to this, suffer the tendency to be bent when worn. This results in performance degradation in terms of resonant frequency shift, which is caused by the changes in the electrical length. Secondly, this is more detrimental for a CP antenna, as the bending distorts the beam and polarization of the antenna [20]. The dual-band antenna is bent using different bending radii in free space to study the effects of bending. Considering different bending radii of the human body, these bending radii are chosen to be 120 mm, 80 mm, and 60 mm for high, upper arm, and wrist of the human body. As depicted in Fig. 8a, the lower band remains intact with the change of the bending radius, whereas the second band shifts downwards with the increase of the bending radius. This observation ascertained the fact that the bending of the antenna changes its electrical length, which shifts its resonant frequency. Moreover, the change in the second band can easily be tuned by altering the U-shape slot, based on the results. Figure 8b proves that the effect on AR plot of the antenna. AR plot is still below 3 dB limit except, the minimum AR value (AR_{min}) changes with different bending radii.

It can be observed from Fig. 8 that bending at a radius of 120 mm has minimal effect on the return loss and axial ratio plot of the antenna in comparison to the flat case. The

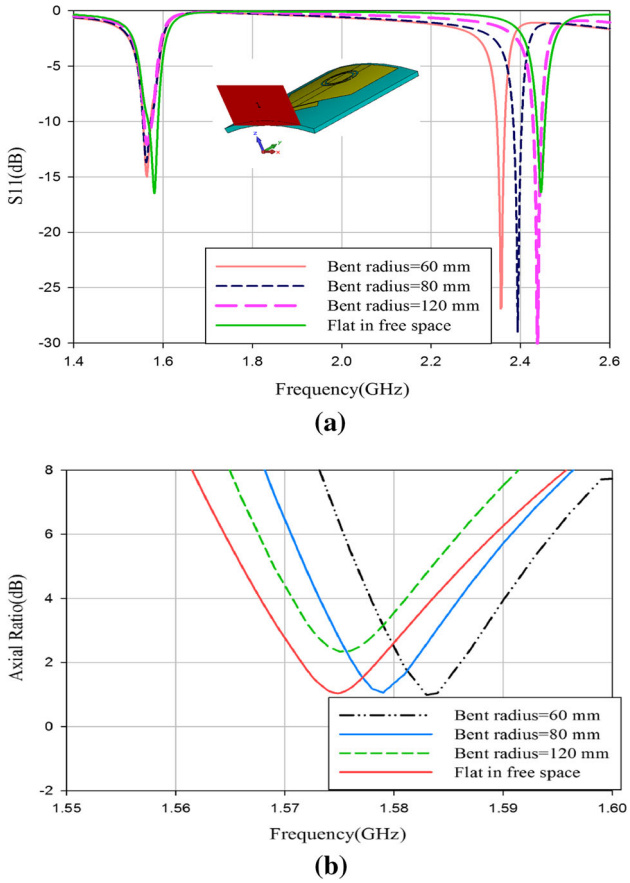

Fig. 8 Effect of bending of dual-band design in free space on **a** S_{11} (dB), **b** Axial Ratio(AR)

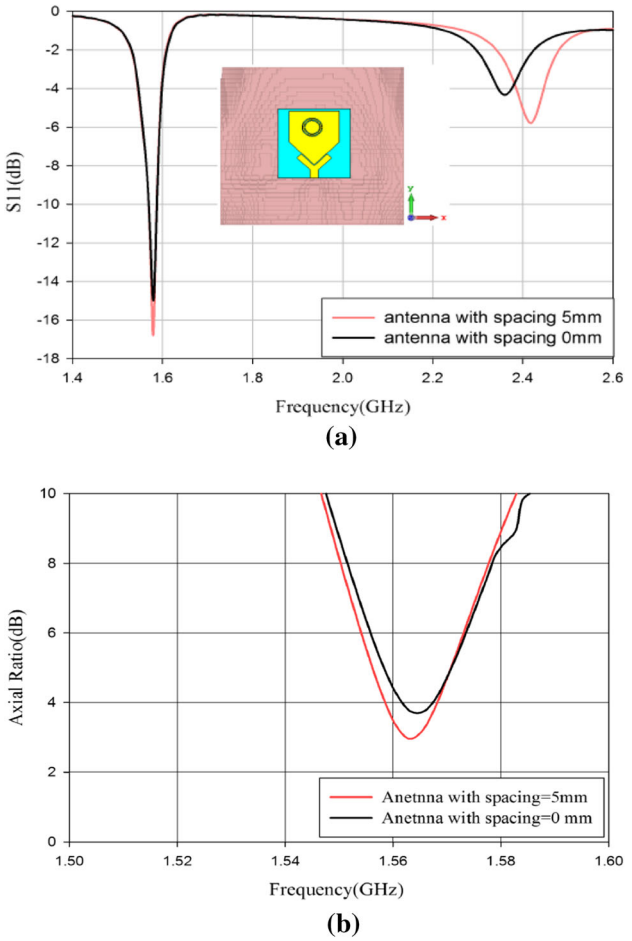

Fig. 9 Antenna's Comparison when kept over upper torso of VOXEL human model at 0 mm and 5 mm from the body: **a** S11 (dB), **b** Axial Ratio(AR)

highest shift in AR_{min} (at 1.583 GHz) is observed for the bending radius of 60 mm. On the contrary, the reflection coefficient is shifted downwards to 2.357 GHz (2.5%) compared to the flat case (at 2.45 GHz), which is considered the worst case for this radius. Hence, this verifies that the dual-band antenna conformally with the device working in free space for indoor/outdoor communication, with slight minimal detuning for when bent with different radii.

3.2 Human Proximity Effects

The dual-band antenna is expected to be detuned under the proximity of human phantoms, mainly causing a shift of the resonance band of the design, besides affecting the total efficiency. In more severe cases, this interaction can significantly change the operating band of the antenna [21]. The antenna is kept at 0 mm and 5 mm from the truncated upper torso (chest) of a male adult voxel human model, Gustav, to investigate the human body effect. Gustav represents a 38-year-old male with a height of 176 cm and weighs 69 kg. The model has been truncated to optimize simulation resources to a size of 20.8 cm × 20.8 cm × 2 cm. It can be seen in Fig. 9a that the reflection coefficient with the human body proximity affects the antenna performance. The antenna maintained operation within the GPS band due to its unidirectional radiation and good isolation against the human body. Its resonance only changed slightly to 1.578 GHz. Despite this, the CP property of the antenna in this lower band is affected, with its AR slightly exceeding 3 dB when placed on the voxel model with the smallest spacing of 0 mm, and returned to below 3 dB at 1.567 GHz when this spacing is increased to 5 mm. On the contrary, in the upper band, it ceased to operate due to its bidirectional pattern in this band, resulting in a strong coupling with the body.

4 SAR Evaluation

Due to the high potential coupling of this antenna with the physical body, the antenna is further assessed by means of SAR (specific absorption rate) only in the lower band. The maximum SAR value averaged over 10 g of tissue is calcu-

Table 2 The comparison with different multi-band antennas for wearable application

Ref	Size	S11%BW	Material	Max gain	HPBW /ARBW	AR Ratio	Application/drawback
[7]	Diameter = $0.504\lambda_0$ Area = $(0.798\ \lambda_0{}^2)$ Height = 4 mm $(0.021\ \lambda_0)$	1.566–1.584 GHz(1.143%) 2.440–2.472 GHz(1.302%)	Rigid substrate ($\varepsilon_r = 2.2$)	0.7dBi at1.575 GHz 1 dBi at2.45 GHz	100^0/N.A	N. A	GPS/WLAN Applications Coaxial Feeding
[1]	$0.524\lambda_0 \times 0.524\lambda_0 \times$ $0.017\ \lambda_0$ Area = $(0.274\ \lambda_0{}^2)$	1.566–1.584 GHz (1.14%)	Rigid substrate ($\varepsilon_r = 10$)	3.03 dBi	N.A/105^0	1.572–1.577 GHz (0.2%)	GPS only
[4]	$0.66\lambda_0 \times 0.69\lambda_0 \times$ $0.016\ \lambda_0$ Area = $(0.45\lambda_0{}^2)$	1.9, 3.3, 3.9, 4.2 GHz	Rigid substrate ($\varepsilon_r = 4.4$)	− 0.1 dBi 1.9 GHz, − 0.8 dBi, 1.5dBi at 3.3 Ghz and 3.9GHZ	N.A	N.A	Wearable application
[5]	$0.49\lambda_0 \times 0.49\lambda_0$x $0.016\ \lambda_0$	2.41–2.5 GHz (3.732%)	Rigid	3.26 dBi	94.2^0/N.A	2.433–2.458 GHz(1.02%	WLAN
[9]	$0.48\lambda_0 \times 0.48\lambda_0$x $0.015\ \lambda_0$ Area = $(0.23\ \lambda_0{}^2)$	1.563–1.583 GHz(1.28%)	Felt	8.26 dBi on head phantom	N.A	1.554–1.586 GHz(2%)	Complex fabrication using shorting pins
[17]	$0.49\lambda_0 \times 0.44\lambda_0$x $0.015\ \lambda_0$ Area = $(0.218\lambda_0{}^2)$	1.33 GHz(3.62%) 2.69 GHz(3.32%)	FR4	1.058 dB	NA	NA	Wearables
Proposed[15]	$0.37\lambda_0 \times 0.40\lambda_0$x $0.016\ \lambda_0$ Thickness = 3.11 mm Area = $(0.148\ \lambda_0{}^2)$	1.564–1.593 GHz (1.837%) 2.439–2.457 GHz (0.735%)	RO3003C ($\varepsilon_r = 3$), Semi-Flexible	3 dBi at 1.575 GHz 1.53dBi at 2.45 GHz	Phi = 0^0 $98.1^0/121^0$ Phi = 90^0 $92.4^0/165^0$ at 1.575 GHz 95.1^0/N.A Phi = 0^0 60.9^0/N.A Phi = 90^0 at 2.45 GHz	1.569–1.581 GHz(0.699%	Wearable for GPS and WLAN

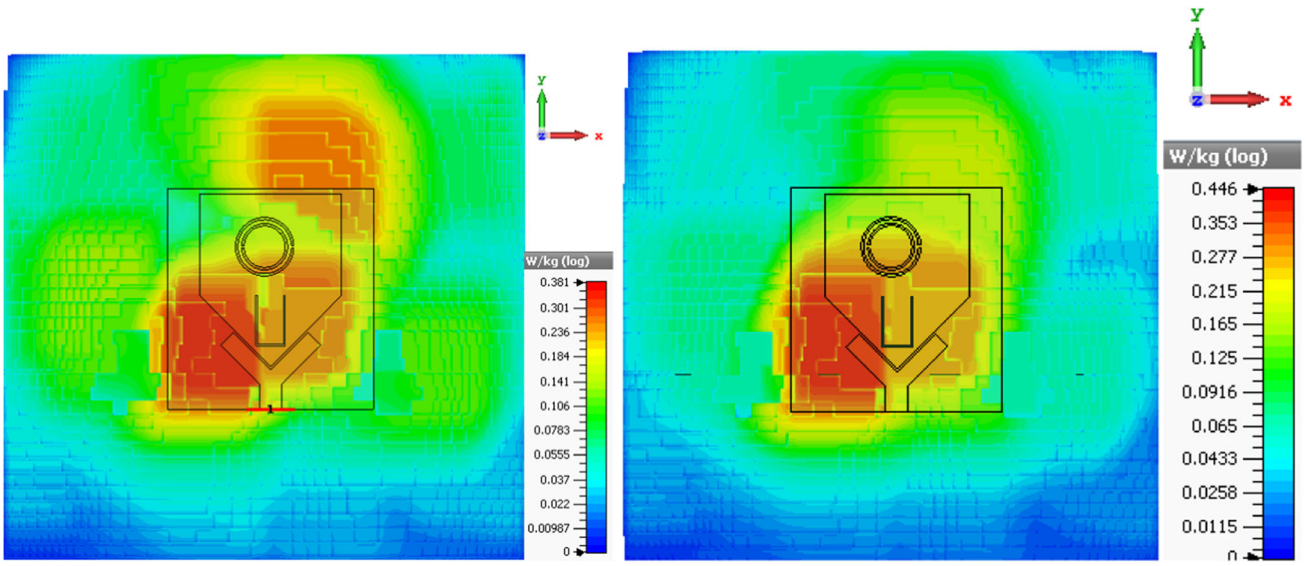

Fig. 10 SAR distribution of the antenna over the upper torso of the human voxel model for different spacing at 1.575 GHz: **a** 0 mm, **b** 5 mm

lated in CST simulation using the same voxel model when the antenna is positioned on the chest when placed at distances of 0 mm and 5 mm. The distance of 5 mm represents the standard clothing thickness and the air gap in practice. The input power to the antenna is set to be 0.5 W (rms), and the SAR was calculated based on the IEEE/IEC 6270–1 standard, averaged over 10 g of biological tissue. Its SAR distributions are shown in Fig. 10. As the spacing increases from 0 to 5 mm, the maximum averaged SAR decreased from 0.446 to 0.381 W/kg (14.6%) at 1.575 GHz. These values are well below the International Commission on Non-Ionizing Radiation Protection (ICNIRP) limit of 2 W/kg averaged over 10 g of human tissue and ensures that the antenna is not posing any health issues to the wearer body. Moreover, the lesser the SAR values, the more it is good for antenna radiation performance. Since, the antenna does not resonate below 10 dB at the upper band, as shown in Fig. 9, its SAR assessment has not been done. The antenna has been compared with other works available in the literature for GPS and WLAN applications in Table 2.

5 Conclusion and Future Directions

In this research article, the extensive analysis of the metamaterial-based multiband antenna along with its parametric study with design equations and equivalent circuit model has been presented. The antenna covers the GNSS L1/E1 lower band centered at 1.575 GHz and the upper WLAN band at 2.45 GHz. Design equations of the antenna have been evaluated and compared with simulated results. An equivalent circuit model of the antenna is proposed along with a parametric study. The proposed equivalent model has two parallel RLC (resistor-inductor-capacitor) circuits connected in series with one capacitor. The optimized circuit model shows good agreement with the proposed design. It is shown that both tank circuits in series with capacitors can be tuned to control lower and upper bands separately. Furthermore, the design equations of CSRR have been presented with an explanation of its different parameters that contributes to the generation of the CP behavior of the antenna. The antenna-maintained operation within the GPS band due to its unidirectional radiation and good isolation against the human body. Like the spacing of the antenna from VOXEL human model increases from 0 to 5 mm, the maximum averaged SAR decreased from 0.446 to 0.381 W/kg (14.56%) at 1.575 GHz with its resonance only changed slightly to 1.578 GHz. Moreover, the CP property of the antenna in this lower band is affected, with its AR slightly exceeding 3 dB when placed on the voxel model with the smallest spacing of 0 mm, and returned to below 3 dB at 1.567 GHz when this spacing is increased to 5 mm. Finally, the antenna has been compared with other standalone solutions for wearable applications to show the compactness of the structure.

For future work, a simple polarization reconfigurable antenna can be designed with the help of presented design equations and analysis of equivalent circuit model. Since the position of the slits in the split ring resonators has an impact on the polarization behavior of the design. If the circular slits inside CSRR are cut in the reverse direction of the proposed antenna, the antenna will give LHCP features instead of RHCP. Our future work will focus on the design of polarization reconfigurable antenna such as by changing switch at the slit positions, the antenna could be made to give LHCP features instead of RHCP.

References

1. So, K.K.; Wong, H.; Luk, K.M.; Chan, C.H.: Miniaturized circularly polarized patch antenna with low back radiation for GPS satellite communications. IEEE Trans. Antennas Propag. **63**, 5934–5938 (2015)
2. Zhang, K.; Soh, P.J.; Yan, S.: Meta-wearable antennas—a review of metamaterial based antennas in wireless body area networks. Materials **14**, 149 (2021)
3. Shome, P.P.; Khan, T.; Laskar, R.H.: A design of U-Shaped slot antenna with broadband dual circularly polarized radiation. Microw. Opt. Technol. Lett. **62**, 2919–2929 (2020)
4. Abdalla, M.A.; Wahba, W.W.; Elreagaily, H.; Allam, A.; Hu, Z.: Miniaturized uni-planar CSRR based quad-band antenna-analysis and investigation. Analog Integr. Circuits Signal Process. **108**, 37–44 (2021)
5. Torres, A.E.; Marante, F.; Tazón, A.; Vassallo, J.: New microstrip radiator feeding by electromagnetic coupling for circular polarization. AEU—Int. J. Electron. Commun. **69**, 1880–1884 (2015)
6. Sabban, A.: New compact wearable metamaterials circular patch antennas for IoT, medical and 5G applications. Appl. Syst. Innov. **3**, 42 (2020)
7. Liu, Y.; Li, X.; Yang, L.; Liu, Y.: A dual-polarized dual-band antenna with omni-directional radiation patterns. IEEE Trans. Antennas Propag. **65**, 4259–4262 (2017)
8. Ghaffarian, M.S.; Moradi, G.; Mousavi, P.: Wide band circularly polarised slot antenna by using artificial transmission line. IET Microw. Antennas Propag. **11**, 672–679 (2017)
9. Lee, H.; Tak, J.; Choi, J.: Wearable antenna integrated into military berets for indoor/outdoor positioning system. IEEE Antennas Wirel. Propag. Lett. **16**, 1919–1922 (2017)
10. Sabran M. I., Rahim S. K. A., Soh P. J., Leow C. Y., Vandenbosch G. A., A simple electromagnetically fed circularly-polarized circular microstrip antenna, *Appl. Comput. Electromagn. Soc. J.,* vol. 30, 2015
11. Bilotti, F.; Toscano, A.; Vegni, L.; Aydin, K.; Alici, K.B.; Ozbay, E.: Equivalent-circuit models for the design of metamaterials based on artificial magnetic inclusions. IEEE Trans. Microw. Theory Tech. **55**, 2865–2873 (2007)
12. Manoharan, S.; Ramasamy, P.; Singaravelu, R.: A quad-band fractal antenna with metamaterial resonator-backed ground for sub-6 GHz, C and X band applications. Appl. Phys. A **127**, 703 (2021)
13. Le, T.T.; Yun, T.Y.: Wearable dual-band high-gain low-SAR antenna for off-body communication. IEEE Antennas Wirel. Propag. Lett. **20**, 1175–1179 (2021)
14. Paracha, K.N.; Rahim, S.K.A.; Soh, P.J.; Khalily, M.: Wearable antennas: a review of materials, structures, and innovative features for autonomous communication and sensing. IEEE Access **7**, 56694–56712 (2019)
15. Paracha, K.N.; Rahim, S.K.A.; Soh, P.J.; Kamarudin, M.R.; Tan, K.G.; Lo, Y.C., et al.: A low profile, dual-band, dual polarized antenna for indoor/outdoor wearable application. IEEE Access **7**, 33277–33288 (2019)
16. Liu, X.Y.; Wu, Z.T.; Fan, Y.; Tentzeris, E.M.: A miniaturized CSRR loaded wide-beamwidth circularly polarized implantable antenna for subcutaneous real-time glucose monitoring. IEEE Antennas Wirel. Propag. Lett. **16**, 577–580 (2017)
17. Malallah, R.E.; Shaaban, R.M.; Al-Tumah, W.I.A.G.: A dual band star-shaped fractal slot antenna: design and measurement. AEU Int. J. Electron. Commun. **127**, 153473 (2020)
18. El Gharbi, M.; Martinez-Estrada, M.; Fernández-García, R.; Ahyoud, S.; Gil, I.: A novel ultra-wide band wearable antenna under different bending conditions for electronic-textile applications. J. Textile Inst. **112**, 437–443 (2021)
19. Almohammed, B.; Ismail, A.; Sali, A.: Electro-textile wearable antennas in wireless body area networks: materials, antenna design, manufacturing techniques, and human body consideration—a review. Textile Res. J. **91**, 646–663 (2020)
20. Rizwan M.; Sydänheimo L.; Ukkonen L., Impact of Bending on the Performance of Circularly Polarized Wearable Antenna, In *Proc. Prog. Electromagn. Res. Symp.*, 2015, pp. 732–737
21. Saha P.; Mitra D.; Parui S. K., Control of Gain and SAR for Wearable Antenna Using AMC Structure, *Radioengineering,* vol. 30, 2021